Use of PP-IGBTs in VSC Medium Voltage Drives Application

Design Summary

Voltage Source Converter (VSC) Medium Voltage (MV) drives play an important role in many areas, and fully controllable power switches, usually IGBTs, are essential devices for the power stage of MV drives. PP-IGBT is a specialty IGBT with high reliability and power density. PP-IGBT based MV drives are the backbone for various critical applications such as marine propulsions, offshore wind turbines, gas compressors, and steel mills.

In this application note, we review a selection of common and emerging topologies for MV drives, followed by a study of the structure and features of PP-IGBT. Additionally, we present the design, analysis, and testing process of a 3L-NPC MV drive using PP-IGBTs with a rating of 6.6k V/16 MVA, which serves as a good example for development of similar converters.

Contact Information

For more information on the topic of PP-IGBTs in MV Drives applications, contact the Littelfuse Power Semiconductor team of product and applications experts:

- PowerSemiSupport@littelfuse.com

Table of Contents

List of Figures

List of Tables

1. Introduction

Voltage source converter/inverter (VSC/VSI) medium voltage (MV) drives are widely used in many areas such as oil and gas, metallurgy, mining, marine drives, energy, and water treatment. Belonging to the Variable Speed Drive (VSD), also known as Adjustable Speed Drive (ASD) category, VSC MV drives can vary the speed/frequency and the torque of an electric machine. As a result, they can:

- Improve efficiency and reduce power consumption of applications/processes (pumps, fans, compressors)
- Minimize the motor inrush current when starting, and
- Offer more precision and optimization of process control

Topologies of MV drives have seen continuous innovations, from the classic three level neutral point clamped converter (3L-NPC), to its variants such as active neutral point clamped converter (ANPC) and cascaded NPC, to the latest Modular Multilevel Converter (MMC) technology. Common voltage grades of MV drives are 2.3 kV, 3.3 kV, 4.16 kV, 6 kV, 6.6 kV, 10 kV, and 11 kV and the output power ranges from sub MW to over a hundred MW.

An Insulated-Gate Bipolar Transistor (IGBT), a fully controllable power switch, is the workhorse for VSC MV drives. Press-pack IGBT (PP-IGBT) is a high-reliability version of IGBT, featuring longer lifetime, high current and power density, hermetic package, and Short Circuit Failure Mode (SCFM). The construction of these devices is totally free from bonding wires and solder bonds, which eliminates the problems of mechanical fatigue associated with conventional Plastic Module IGBT (PMI). Consequently, MV drives based on PP-IGBT are normally used in applications that have heavy and volatile loads, and/or work in hostile or extreme environments; for instance, marine propulsion, oil and gas compressor and station, offshore wind turbine, steel mill, and similar applications.

This application note starts with a brief review of frequently used topologies for VSC MV drives, and then describes PP-IGBT in detail by reviewing its internal structure and comparing it with competing power switches. To gain an insight into the development of MV drives using PP-IGBT, the design, analysis, and testing process of a 3L-NPC with a rating of 6.6 kV/16 MVA will be discussed as a case study.

2. Typical Multilevel Converter Topologies for VSC MV Drives

Numerous topologies are used in the market for VSC MV drives, and only typical ones are introduced here. The purpose is to explain the fundamentals of topologies for MV drives; therefore, mainly three-level converters are used to exemplify basics of multilevel converters for MV drives.

2.1. Neutral-Point Clamped Converter

The Neutral-Point Clamped (NPC) converter is one of the most commonly used topologies for MV drives, especially the 3L-NPC converter. Figure 1 illustrates the topology of 3L-NPC, in which the output levels of each phase are center-point (neutral) referenced through clamping diodes and switches. In each phase logically there are four switches and two clamping diodes, and the diodes directly connect to the neutral-point of the DC-link.

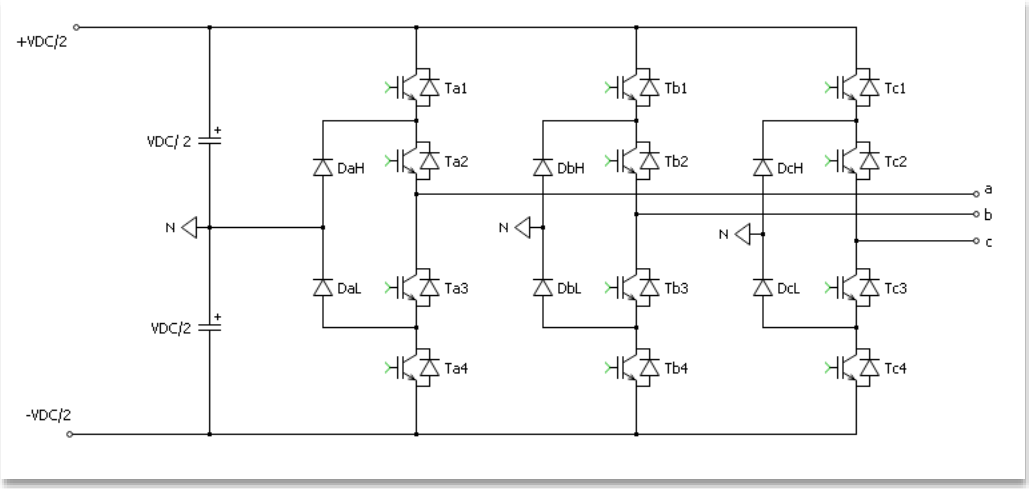

Figure 1. Three-Level Three Phase NPC Topology

The output of each phase has three finite output states: $+V_{DC}/2$, 0, and $-V_{DC}/2$, by referring to the neutral point of the DC-link. For instance, for Phase a in Figure 1, when T_{a1} and T_{a2} are ON, the Phase a output terminal will be shorted to the highest potential of the DC-link and thus the output voltage will be $+V_{DC}/2$; when T_{a2} and T_{a3} are ON, the Phase a output terminal will be shorted to the neutral point of the DC-link and the output voltage will be 0; when T_{a3} and T_{a4} are ON, the Phase a output terminal will be shorted to the lowest potential of the DC-link and the output voltage will be $-V_{DC}/2$. These permitted combinations of switch status and corresponding output voltages are summarized in Table 1 [1], and it is evident that switch status of T_1 vs T_3 and T_2 vs T_4 are always exclusive. In addition, due to concerns about high losses and unequal dynamic voltage on each switch, direct switching of output states between $+V_{DC}/2$ and $-V_{DC}/2$, which will involve commutation of all switches at the same time, is not allowed.

Table 1. 3L-NPC Switching States and Equivalent Phase Output Voltage (1 for ON & 0 for OFF)

Phase Output Voltage, V_{aN}	Switching Device			
	T_{a1}	T_{a2}	T_{a3}	T_{a4}
$V_{DC}/2$	1	1	0	0
0	0	1	1	0
$-V_{DC}/2$	0	0	1	1

As illustrated in Figure 2, for the line output voltage of 3L-NPC, there are five finite states in total: V_{DC}, $+V_{DC}/2$, 0, $-V_{DC}/2$, and $-V_{DC}$. The switch status for V_{DC}, $+V_{DC}/2$ and 0 are shown in sub-figures of Figure 3 respectively, where the current path will go through the associated devices with ON status.

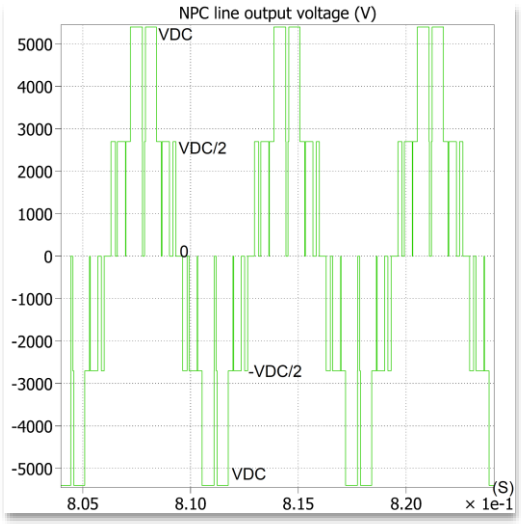

Figure 2. Waveforms of Line Output Voltage of 3L-NPC (DC Link ±2.7 kV)

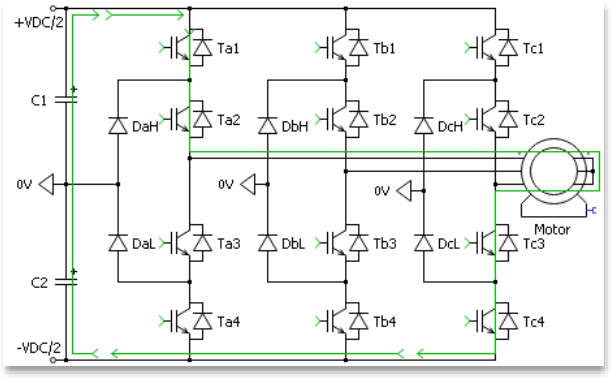

(a) V_{DC}

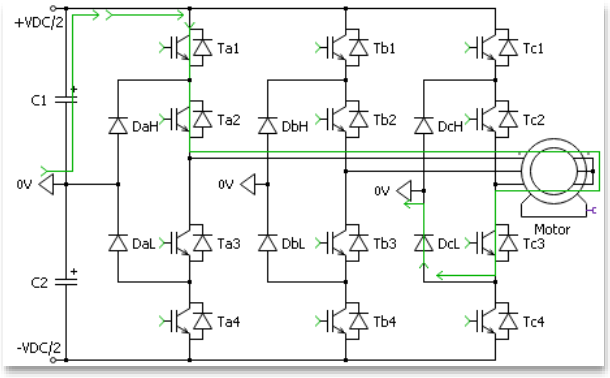

(b) $V_{DC}/2$

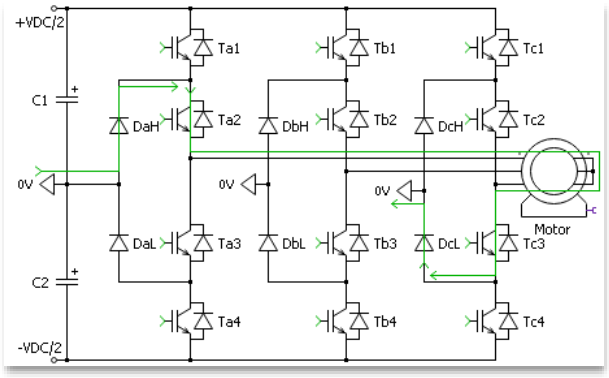

(c) 0

Figure 3. Line Output Voltage, Current Paths and Associated Conduction Devices

2.2. Active Neutral-Point Clamped Converter

Despite the wide application of 3L-NPC topology for MV drives, its main drawback is the loss distribution imbalance among power devices. For instance, when a 3L-NPC converter works in the inverter mode, normally the outer switches, namely T_1 and T4 in Figure 1, will generate much higher losses than the inner switches, namely T_2 and T3 in Figure 1. The switches that generate more losses will be the bottleneck for the whole converter, and such imbalance of losses will limit the capacity of the converter.

To cope with the issue of uneven power loss distribution of the NPC topology, the Active Neutral-Point Clamped (ANPC) topology has been developed. The topology of a three phase three-level ANPC converter (3L-ANPC) is illustrated in Figure 4. As a modified version of 3L-NPC topology, the clamping diodes are replaced by controllable switches. Moreover, like the 3L-NPC, there are four controllable switches on the main branch of each phase leg.

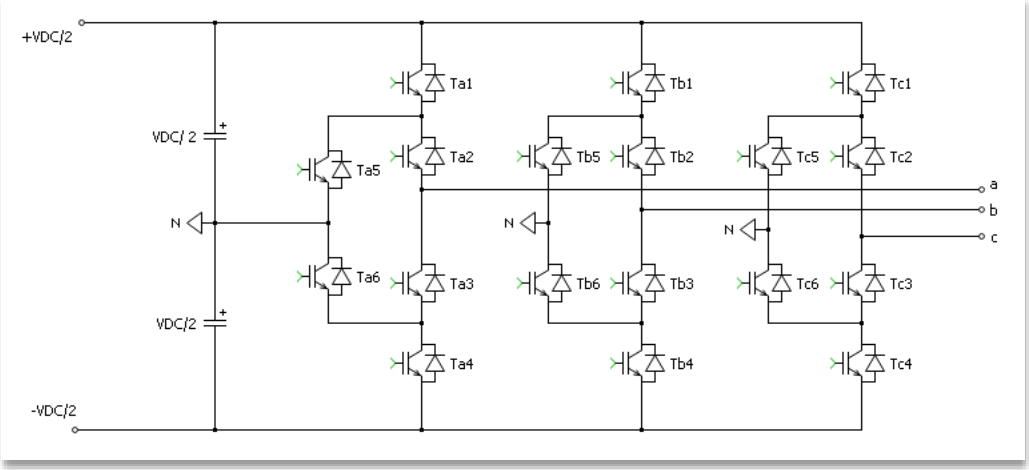

Figure 4. Topology of a 3L-ANPC Converter

In total, there are six switching states for each phase of a 3L-ANPC, which are listed in Table 2 [2], [3]. Thanks to the controllable switches in the clamping circuit, ANPC has four redundant states to create output voltage level zero. As shown in Figure 5, no matter the direction of the load current, there are always two current paths available that lead to the neutral point of the converter. These redundant states can be used to redistribute switching losses equally during commutation by selecting the suitable state for the switches. As a result, with the same DC-link voltage level and same ratings of power switches, ANPC can normally produce higher output power or operate with higher switching frequency than NPC, with associated increases in cost of additional power switches used, hardware, and modulation complexity.

Table 2. 3L-ANPC Switching States and Equivalent Phase Output Voltage

Phase Output Voltage V_{aN}	Switching Device					
	T_{a1}	T_{a2}	T_{a3}	T_{a4}	T_{a5}	T_{a6}
$V_{DC}/2$	1	1	0	0	0	1
0	0	1	0	0	1	0
0	0	1	0	1	1	0
0	1	0	1	0	0	1
0	0	0	1	0	0	1
$-V_{DC}/2$	0	0	1	1	1	0

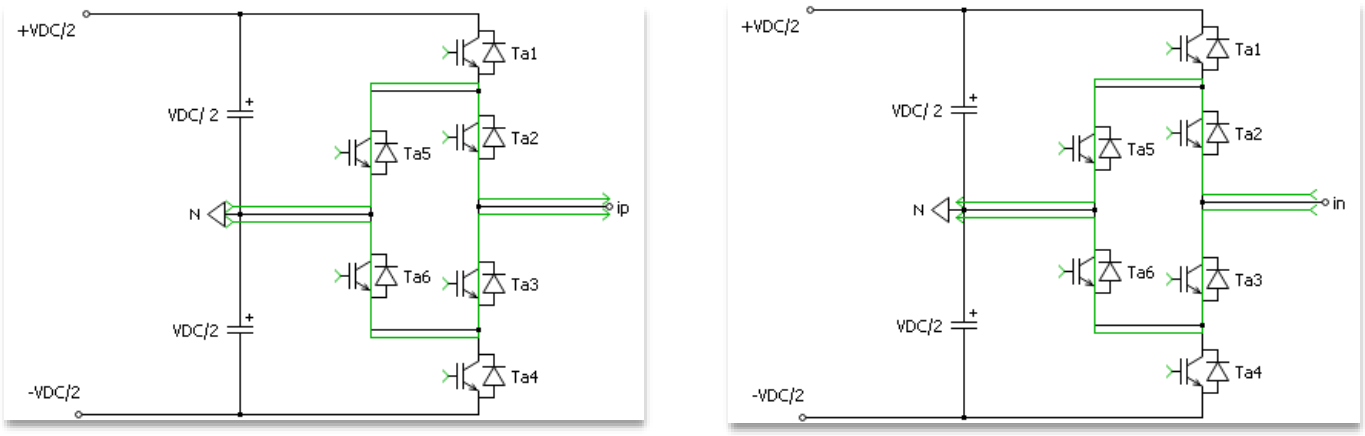

(a) Outgoing (b) Incoming

Figure 5. Current Paths for the Switching States of 0 Phase Output Voltage

2.3. T-type Converter

The T-type converter is also known as Neutral Point Piloted (NPP) converter or Transistor Clamped Converter (TCC). It is an alternative to the ANPC converter and can deal with the issue of loss imbalance among power switches of an NPC converter. Figure 6 shows a typical three-level T-type converter using 4.5 kV PP-IGBT, which will produce 3.3 kV rms line output voltage if the total DC-link V_{DC} is 5 kV. The phase leg switches are built from two 4.5 kV in series connection. A distinct feature of this topology is the use of an active bidirectional switch to link output terminal of a phase leg to the midpoint of DC-link voltage, and the bidirectional composite switch consists of two controllable power switches in anti-series connection.

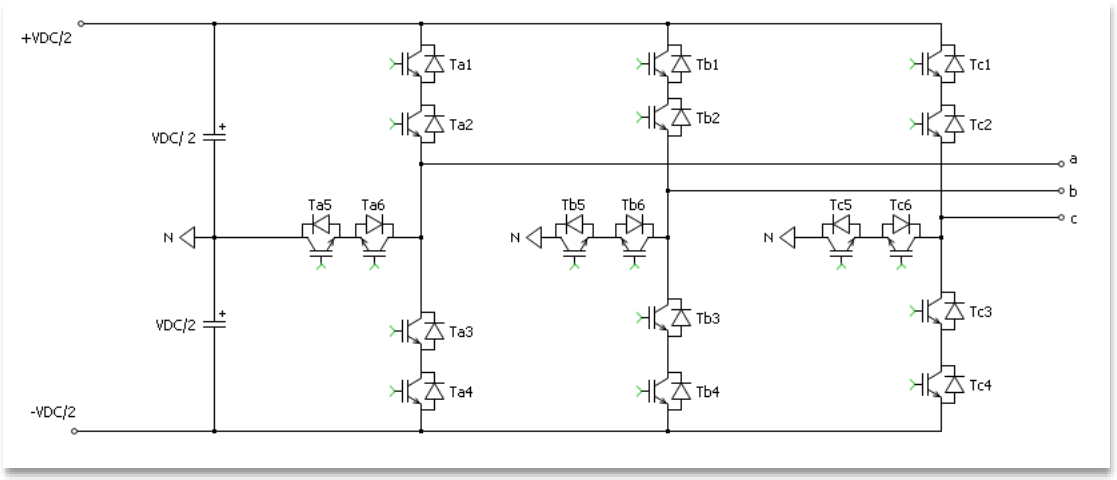

Figure 6. Topology of a Three-level T-type Converter

The working principle of the T-type converter is very straightforward – when power switches T_1 and T_2 are turned ON, the output terminal of a phase leg will be connected to the highest potential $+V_{DC}/2$; when power switches T_3 and T_4 are turned ON, the output terminal of a phase leg will be connected to the lowest potential $-V_{DC}/2$; when power switches T_5 and T_6 are turned ON, the output terminal of a phase leg will be connected to the midpoint of the DC-link. The practical switching states and corresponding output voltage level of a phase leg of a three-level T-type converter is shown in Error! Reference source not found. [4], which allows blank time when switching between $+V_{DC}/2$ or $-V_{DC}/2$ and 0 output voltage.

Table 3. Switching States and Equivalent Phase Output Voltage of a Three-level T-type Converter

Phase Output Voltage V_{aN}	Switching Device					
	T_{a1}	T_{a2}	T_{a3}	T_{a4}	T_{a5}	T_{a6}
$V_{DC}/2$	1	1	0	0	1	0
0	0	0	0	0	1	1
$-V_{DC}/2$	0	0	1	1	0	1

Similar to ANPC, the losses among T_1 ~ T_4 are more uniformly distributed; therefore, with the same DC-link voltage input and same ratings of power switches, the T-type converter can produce higher output power or operate with higher switching frequency. In addition, for T_1 ~ T_4, during current commutation they are only required to withstand $V_{DC}/4$ rather than $V_{DC}/2$, which means that there are larger safety margins for these power switches against their Safe Operating Area (SOA).

2.4. Cascaded H-bridge Converter

The Cascaded H-bridge (CHB) converter is also known as Chain-link H-bridge. As shown in Figure 7, a single H-bridge or full-bridge is a well-known simple structure which can produce three output states: $+V_{DC}$, 0, and $-V_{DC}$. Multiple H-bridge modules can be connected in series as a phase leg, which can produce additional output states. For instance, when two H-bridge modules are connected in series, the resulting phase leg can produce output states of +2 V_{DC}, $+V_{DC}$, 0, $-V_{DC}$ and -2 V_{DC} across its two terminals.

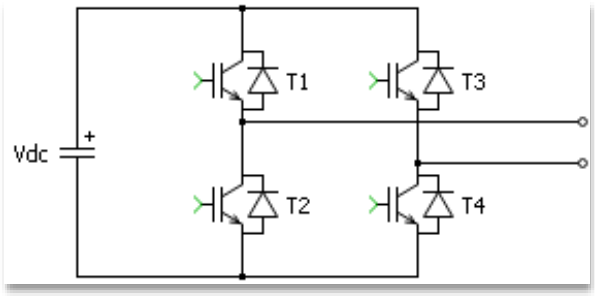

Figure 7. Single H-Bridge

An example of the CHB converter for MV drives is shown in Figure 8 [5]. In this design, three modules are connected in series to form one phase leg, and terminals of phase legs on one side are connected as the common point. The differential voltage between two phase legs, which is the line voltage, can produce output states from -6 V_{DC} to 6 V_{DC} with one V_{DC} as a step.

One H-bridge module is termed as a submodule, or a power module, or a power cell. The front end of a power module in Figure 8 is formed by a six pulse three phase diode bridge. Phase shift of input voltage to power modules in a phase leg is achieved by special arrangement of windings of a transformer on the secondary side, which helps reduce ripples of output voltages.

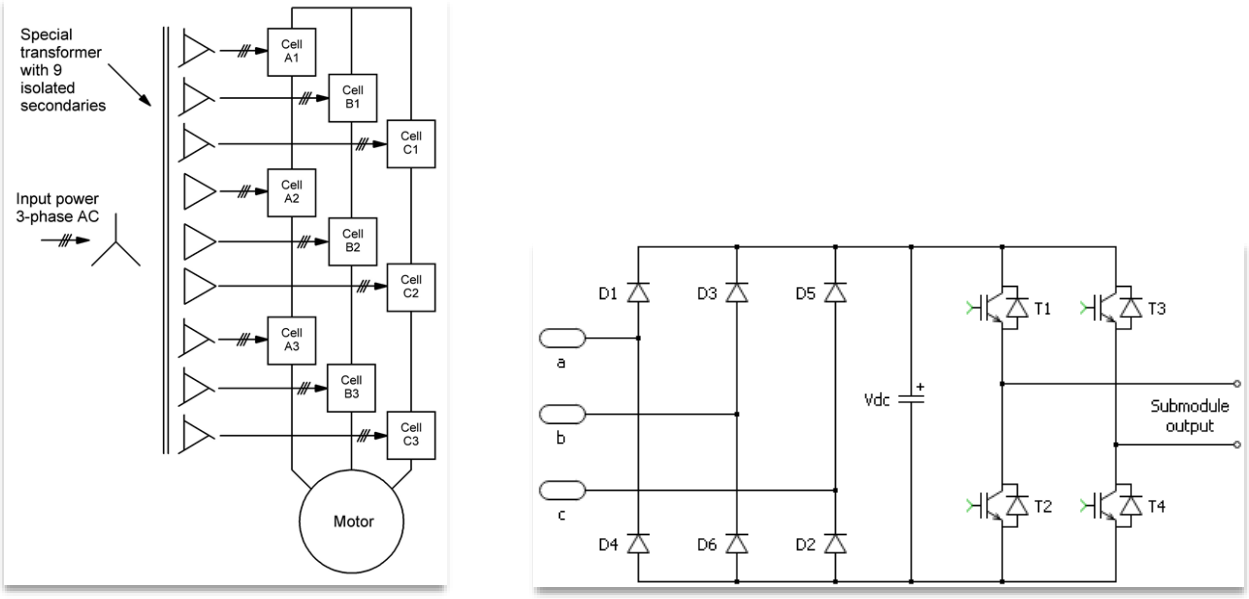

(a) Overall Circuit Schematic

(b) Circuit of a Power Cell

Figure 8. Example CHB Converter

An advantage of the CHB converter is the modular design with distributed DC-link capacitor, which eases the difficulty of hardware design. Other benefits include better output waveforms and low dv/dt due to more output voltage levels and a small step between two levels. On the other hand, the CHB converter requires an isolated DC source, which is often provided with a three-phase transformer (Figure 8). This transformer must have multiple secondary windings that will lead to a bulkier system with more component counts.

2.5. Flying Capacitor Converter

The Flying Capacitor (FC) converter creates multilevel output voltages by using multiple DC capacitors and switches. Figure 9 illustrates the topology of a three-level FC converter. Though it is very similar to that of the NPC converter in Figure 1, the major difference is that the neutral clamping diodes are replaced by capacitors in an FC converter.

For each phase leg of the three-level FC converter in Figure 9, there are four controllable switches T_1~T_4. To avoid short circuit of the capacitors through switches, the switches T_2 and T_3 are paired, switches T_1 and T_4 paired, and gate signals for two paired switches are inverted. When T_1 and T_2 are turned ON, the output terminal of a phase leg will be connected to the highest potential of the DC-link. When T_3 and T_4 are ON, the phase output will be shorted to the lowest potential of the DC-link. When T_1 and T_3 are ON, or when T_2 and T_4 are ON, the phase output will be approximately equal to half of the total DC-link voltage. The output voltage of a phase leg is summarized in Table 4 [1], and an example of line output voltage is shown in Figure 10, which is very similar to that of the NPC in Figure 2.

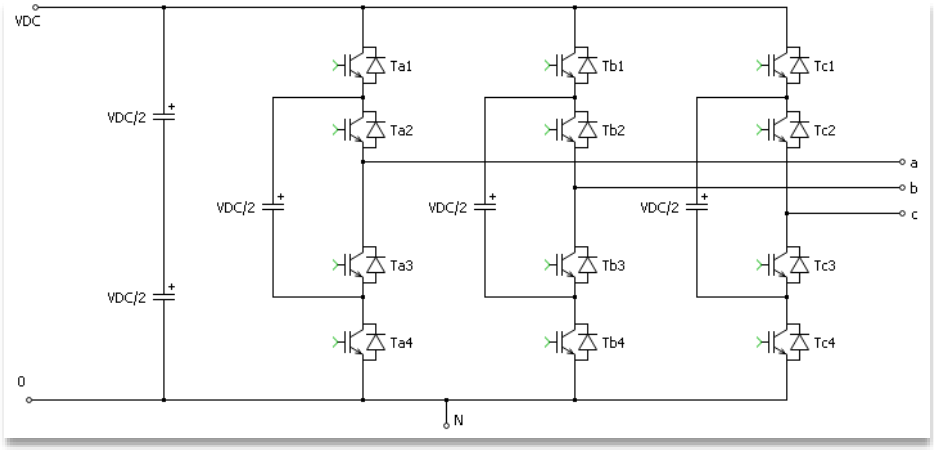

Figure 9. Three-level Flying Capacitor Converter

Table 4. Switching States and Equivalent Phase Output Voltage of a Three-level FC Converter

Phase Output Voltage V_{aN}	Switching Device			
	T_{a1}	T_{a2}	T_{a3}	T_{a4}
V_{DC}	1	1	0	0
$V_{DC}/2$	1	0	1	0
$V_{DC}/2$	0	1	0	1
0	0	0	1	1

The FC converter has a few advantages. Additional capacitors in the converter means more energy storage, which makes the system more capable of dealing with momentary loss of power from the grid. Moreover, the FC converter has a modular configuration, in which the paired switches and corresponding capacitors form a module. Such a modular structure makes it a scalable converter. In addition, it is reported that the FC converter has no problems with voltage sharing between the semiconductor elements and does not need snubber components [6].

On the other hand, the downsides of the FC converter include requirement of large numbers of DC capacitors with separate pre-charge circuits, complex control strategy to keep capacitor voltage in balance for a converter with more than three levels, and high expense of flying capacitor at low and medium switching frequency.

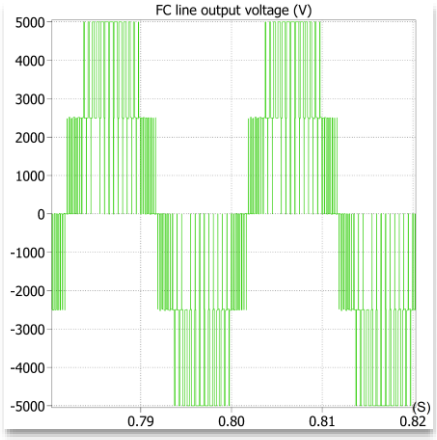

Figure 10. Example of Line Output Voltage of a Three-level FC Converter (DC Link ±2.5 kV)

2.6. Modular Multilevel Converter

Modular Multilevel Converter (MMC) is the current mainstream technology for VSC HVDC, and it's gaining more popularity for MV drive applications. The success of MMC is largely attributed to the modular design concept. Like the CHB, the basic Power Electronic Building Block (PEBB) of an MMC is called a submodule, or a power module, or a cell. Typical topologies of MMC submodule for MV drives include half-bridge, full-bridge and their variants [5], [7].

The basic circuit topology of an MMC with half-bridge submodule is shown in Figure 11 [8]. Gate signals of T_1 and T_2 of a submodule are inverted to avoid short circuit of the DC-link capacitor. When T_1 is ON, the DC-link capacitor voltage of a submodule will be inserted into the phase leg. When T_2 is ON, the two terminals of a submodule will be shorted, and the DC-link capacitor will be disengaged. When both T_1 and T_2 are OFF, the submodule output voltage will depend on current direction. The switching states and corresponding current paths are summarized in Figure 12 and Error! Reference source not found..

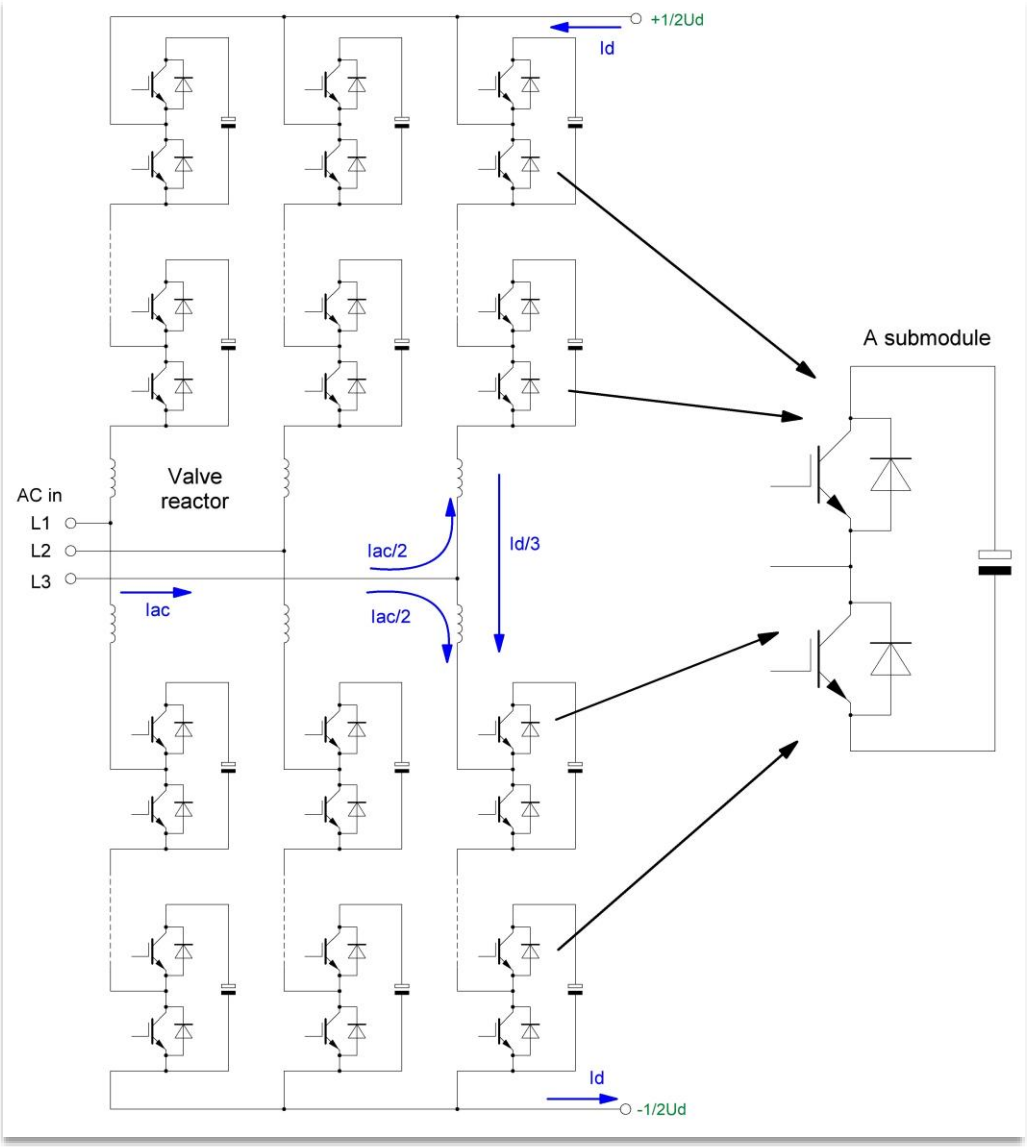

Figure 11. MMC Topology with Half-bridge Submodules

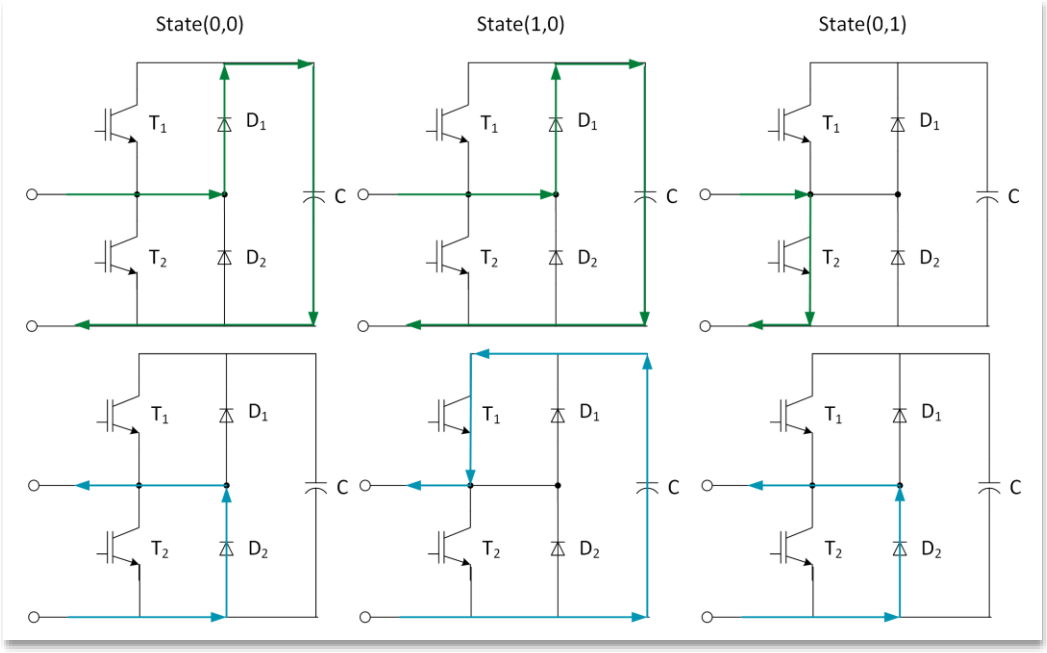

Figure 12. States and Current Paths of a Half-bridge Submodule

Table 5. States and Current Paths of a Half-bridge Submodule

States	Current Direction	Current Path	Output Voltage	Capacitor Voltage
(0, 0) T_1 Off, T_2 Off	Incoming	D_1	1	Charging
	Outgoing	D_2	0	No change
(1, 0) T_1 On, T_2 Off	Incoming	D_1	1	Charging
	Outgoing	T_1	1	Discharging
(0, 1) T_1 Off, T_2 On	Incoming	T_2	0	No change
	Outgoing	D_2	0	No change

MMC has several advantages. Firstly, the modular concept eases the difficulty of hardware design while also making it more scalable. The power stage of a submodule is very straightforward for designers, not only because the half-bridge topology is a well-known simple structure, but also because snubber circuit is not mandatory. Moreover, more voltage steps can be easily obtained, which means good voltage waveforms with fewer harmonics and low dv/dt.

On the other hand, design difficulty has been shifted to control and modulation, in order to keep the voltage of submodule capacitors in balance or within an acceptable range. Moreover, energy storage against converter power rating can be relatively high due to high number of DC-link capacitors.

3. Selection of Power Switch

There are three main groups of power switches that are used for modern VSC MV drives: Plastic Module IGBT and diode (PMI), Press-Pack IGBT and diode (PP-IGBT) and Integrated Gate-Commutated Thyristor (IGCT). Overall, PMI is the most common power switch for MV drives due to its widely availability, ease of mounting, and price. However, for MV drive systems that require extremely high reliability or power density, PMI has its own inherent drawbacks. These include relatively small current capabilities, short lifetime because of solder layer and bonding wire fatigues, non-uniform stray inductance and non-uniform thermal resistance among chips inside a module, small i^2t or thermal withstanding capabilities of diodes for surge conditions, open-circuit failure mode, and non-hermetic and prone-to-rupture package. The press-pack IGBT and diode based converter design can overcome these drawbacks thanks to their high current capabilities, long lifetime due to elimination of solder layer and bonding wires, double-side cooling, more uniform stray inductance and more uniform thermal resistance among chips, hermetic and rupture-resistant package, very high i^2t or thermal withstanding capabilities of diodes for surge conditions, and Short-Circuit Failure Mode (SCFM) feature.

IGCT, based on thyristor technology, has the advantage of low ON-state losses. Like PP-IGBT, IGCT has long lifetime, double-side cooling, SCFM and hermetic package. However, as a thyristor-type device, IGCT is a current-driven switch and requires high power consumption of gate unit. It also needs bulky snubber network for normal operation, and it cannot limit and turn off fault current in case of short circuit. Consequently, the PP-IGBT devices are the optimal choice for high power MV drives with high reliability requirement. Error! Reference source not found. [9] shows a brief comparison among PMI, PP-IGBT, and IGCT power switches.

Table 6. Comparison of Power Switches for MV Drives

Devices	Advantages	Drawbacks
Plastic Module IGBT	• Low power consumption of gate unit • Current limitation in case of short circuit • Many manufacturers • Many voltage ratings	• High-on state losses • Low thermal cycle endurances • Open circuit and risk of explosion if failure
PP-IGBT	• Low power consumption of gate unit • Current limitation in case of short circuit • High thermal cycle endurances • Double-side cooling • Short circuit failure mode	• Complex mechanical assembly
IGCT	• Low on state losses • High thermal cycle endurances • Stable short circuit in case of failure	• High power consumption of gate unit • Use of clamp circuit • No current limitation in case of short circuit

PP-IGBTs' exceptional performance is due to their unique internal structure. Construction of the PP-IGBT is illustrated in Figure 13 and is based on established design concept [10], [11]. Die is individually mounted in cells as shown in Figure 13 (a), which can be pre-tested prior to encapsulation. Each cell comprises a plastic carrier into which the die is mounted between two molybdenum plates, supported in the cell by a silver shim. Contact is made to the gate via a spring-loaded pin which connects both to the die and the distribution board fitted in the lower half of the emitter electrode. The die has a special metallization layer to allow full pressure contact to both the collector and emitter. When the package is closed, the cells are directly mounted between copper electrodes in a fully hermetic package as illustrated in Figure 13 (b) [12].

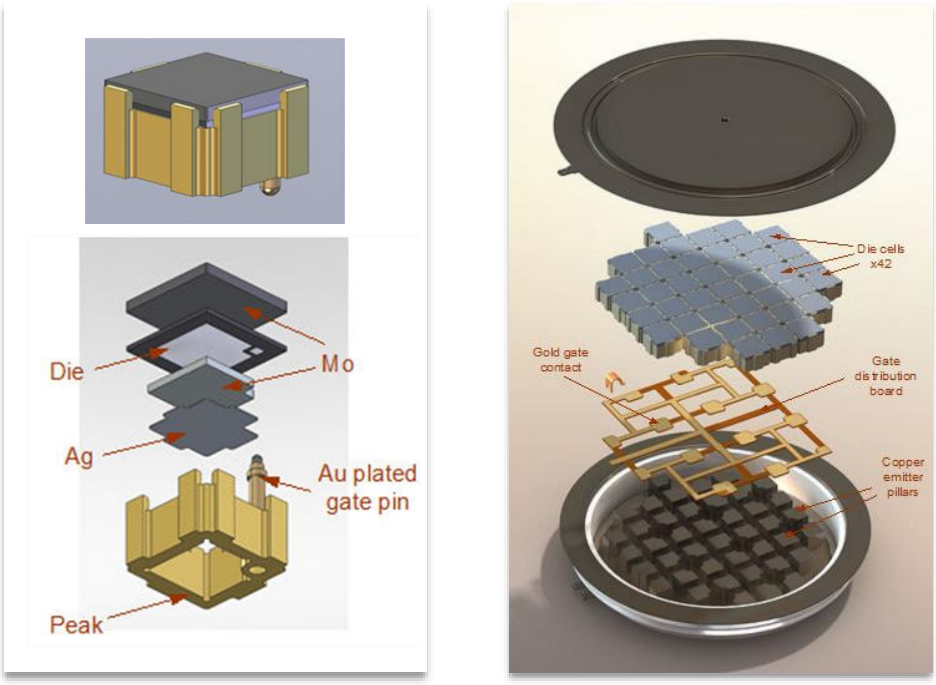

(a) IGBT CellI00 (b) Exploded View of Open Package

Figure 13. Construction of the PP-IGBT

4. Case Study of the Use of PP-IGBT T2000BB45G in 6.6 kV/16 MVA Three-level NPC MV Drives

In this application note, the stack assembly for phase legs of a 6.6 kV/16 MVA MV drives will be developed for a gas station application based on the 3L-NPC topology (Figure 1). The DC-link voltage is rated at ±5 kVDC to produce 6.6 kV RMS line voltage on the AC output. To properly cope with such voltage rating, a logical controllable switch in Figure 1 is realized using two PP-IGBT T2000BB45G in series, which have a rating of 4.5 kV/2 kA with built-in anti-parallel diode [13]; and a logical neutral-point clamping diode in Figure 1 is realized using two power diodes E2400EC45E in series [14]. The structural and cooling design, snubber circuits, electrothermal simulation for the stack assembly, and a selection of tests will be reported.

4.1. Stack Design and Simulation

4.1.1. Structural and Cooling Design

Two sperate stacks are used to form a complete phase leg – one is the PP-IGBT stack (part number XA1600BV45WT) and the other is the clamping diode stack (part number XA1600EV45WE). This arrangement minimizes the stray inductance in the commutation loop and alleviates the difficulties of manufacturing and transportation. Three sets of such phase leg assembly are required to form a 3L-NPC converter, which can produce 6.6 kV/16 MVA output.

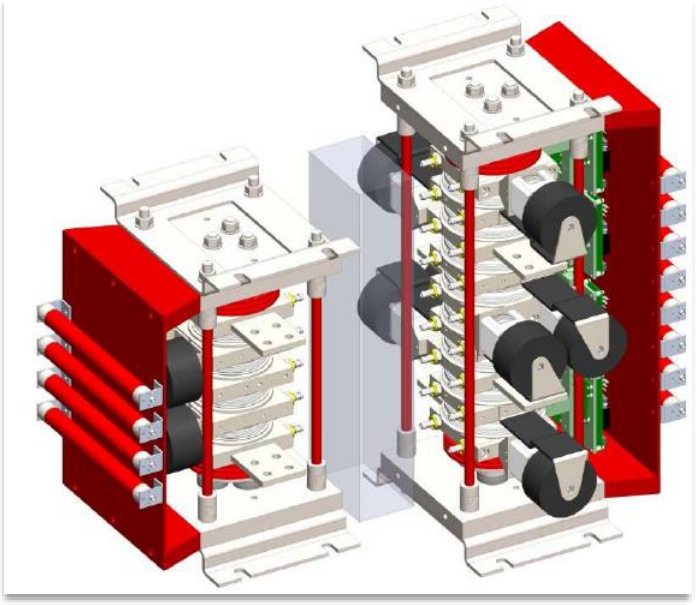

Figure 14. Phase Leg Assembly Consisting of the PP-IGBT and Diode Stacks

In both stacks, the physical positions of power devices are arranged in a straightforward top-down style. For instance, the top switch T_1 in Figure 1 is realized by the top two PP-IGBTs in the IGBT stack. Components of corresponding snubber circuits are attached to both stacks respectively, and gate driver boards are mounted on one side of the IGBT stack. Bus bars of stacks are designed to be an integral part of some coolers/cold plates, rather than adding extra bus bars inside the stack. The bus bars for interconnection of two stacks are located on one side of the stacks (Figure 14 [15] and Figure 28 (b)), and bus bars for DC plus, minus, AC output and DC neutral connections are located on the opposite side of the stacks respectively.

Inside both stacks, a press-pack device is sandwiched by two coolers and vice versa, requiring double-side cooling capabilities for coolers. Additionally, to ensure good current sharing among chips inside a PP-IGBT, a cooler shall be designed to have relatively uniform temperature distribution on its surface. The Computational Fluid Dynamics (CFD) simulation results are shown in Figure 15 which indicate that cooling channels are properly located on both sides of a cooler. These cooling channels will force coolant to flow to the center of a cooler first, and then go out to its outlet. With such an arrangement, cold and hot coolant channels will be adjacent to each other when the coolant travels through a cooler and absorbs power losses. Eventually, it helps to minimize temperature spread on the cooler surface. In the IGBT/diode stacks, the aluminum coolers XW180GA34# are used, and nominal values of their thermal resistance are 0.0038 K/W, with 6 L/M coolant flow rate [16].

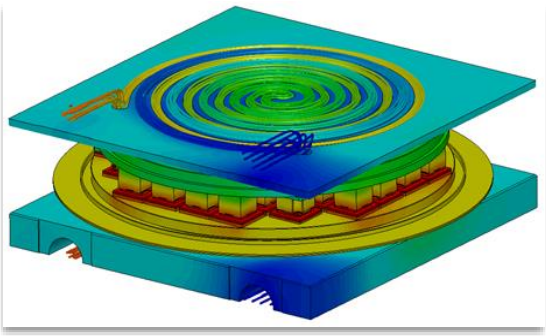

Figure 15. CFD Analysis on Coolers and Devices

For the clamping system, a pre-loaded, 3-point disc spring clamp is used. It comprises a pre-loaded top clamp, set to the required force and a 'free' or 'floating' bottom clamp. This pre-loaded top clamp has a disc spring indication to allow for quick and easy maintenance. The bottom clamp enables the two halves of the clamp to provide parallel clamping of the assembly, while also allowing for thermal expansion during the operation of the assembly. Overall clamping provides an accurate and even force distribution throughout the unit which is critical to ensure the IGBT device can operate to its maximum potential [17].

4.1.2. Snubber Design

RCD and RC snubber circuits are used for IGBTs and clamping diodes respectively. The RCD snubber circuit of an IGBT is used to reduce its turn-off overvoltage and losses, and it also enhances dynamic voltage sharing between power devices. During the IGBT turn-off process, the IGBT current is normally commutated to the RCD snubber with a high di/dt; and when voltage of the snubber capacitor is higher than the DC-link voltage, the snubber diode is quickly reverse biased, which results in diode reverse recovery with a very high di/dt. Therefore, a very fast diode is required for the snubber circuit. For this application, a high sonic diode E0460EC45E that has a voltage rating of 4.5 kV and di/dt rating of -1000 A/µs, is used as the snubber diode with a compact box clamp [14], [18]. The diode module is mounted on an aluminum spacer that is attached onto a cooler, and a 0.33 µF, 4 kV voltage grade snubber capacitor [17] is further mounted on the diode module (Figure 14). In addition, a direct water-cooled 1700 W resistor is used for the RCD snubber, and static sharing resistors are used due to the involvement of series operation of power devices.

4.1.3. Electrothermal Simulation

Electrothermal simulations have been performed to evaluate losses and junction temperature of the PP-IGBT T2000BB45G and diode E2400EC45E in this project. A circuit simulation model has been built, which consists of three phase legs and inductive loads for the 6.6 kV/16 MVA 3L-NPC VSI. The circuit diagrams for the whole inverter and individual phase leg are shown in Figure 16 and Figure 17 respectively. In this circuit simulation, the general setup is as follows:

- Inverter working mode
- Output frequency 119 Hz, switching frequency 450 Hz
- DC-link voltage ±5 kV, amplitude modulation ratio 1 with Sinusoidal PWM
- Output line voltage 6,124 V_{rms}
- Power factor 0.81

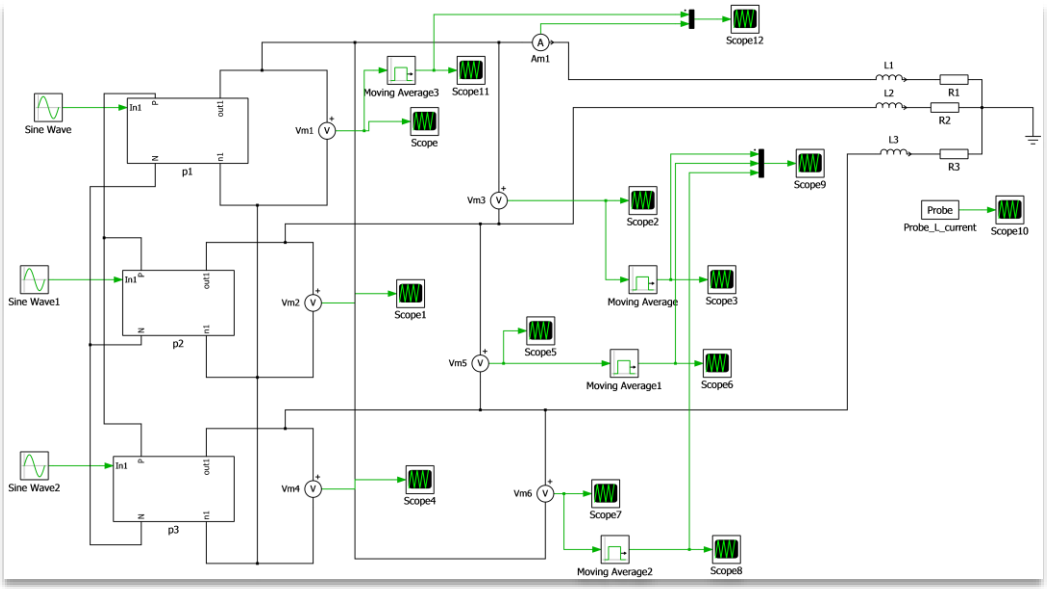

Figure 16. Circuit Diagram for the 3L-NPC VSI (p1~p3 are Phase Legs)

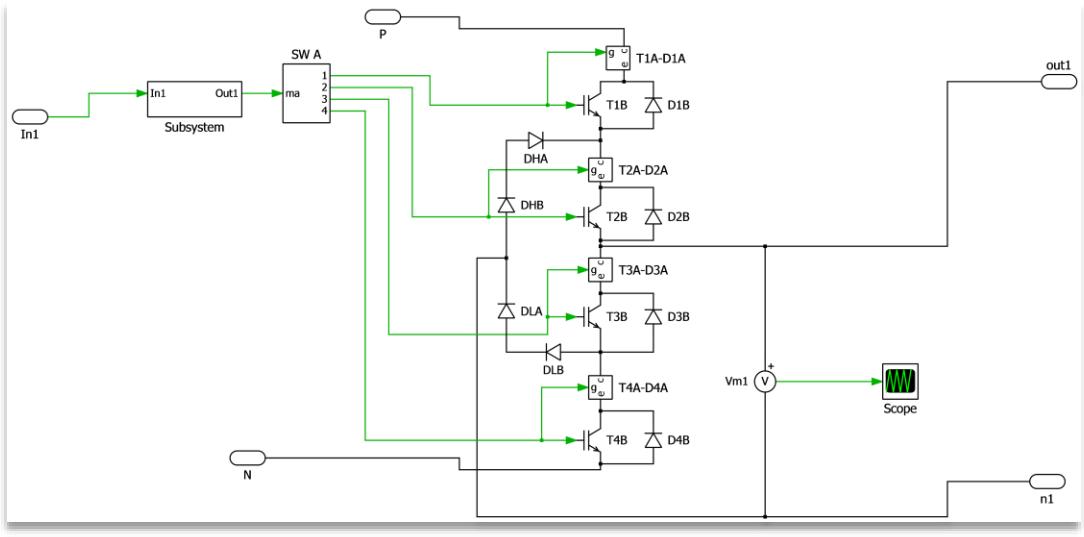

Figure 17. One Phase Leg of the 3L-NPC VSI (T1A-D1A is a Duplicate of the T1B & D1B Pair)

In conjunction with electrical circuit simulation, thermal simulation is carried out simultaneously, based on the power device's electro-thermal models and cooler parameters. As a result, power losses and junction temperature of power devices are calculated continuously. An illustration of an IGBT's electro-thermal model that is used in this simulation is shown in Figure 18. In addition, the general simulation setup is as follows:

- 10% reduction on IGBT turn-off losses considering RCD snubber
- Coolant inlet temperature 40°C
- Cooler thermal resistance for T2000BB45G: 0.0038x125/132°C/W @6LPM coolant flow
- Cooler thermal resistance for E2400EC45E: 0.0038x125/85°C/W @6LPM coolant flow

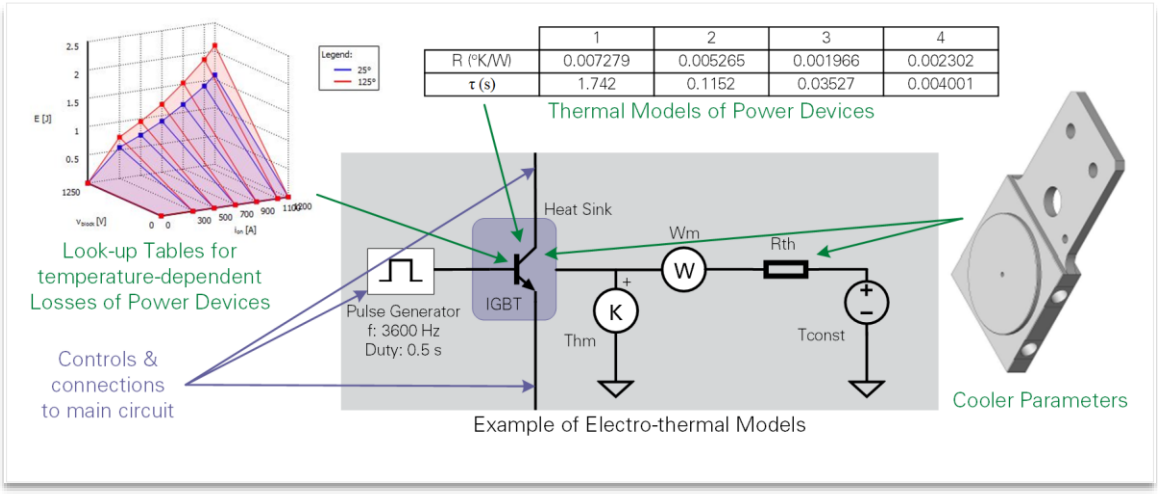

	1	2	3	4
R (°K/W)	0.007279	0.005265	0.001966	0.002302
τ (s)	1.742	0.1152	0.03527	0.004001

Figure 18. Illustration of the IGBT/Cooler Model for Electro-thermal Simulation

The instantaneous inverter output line voltage is shown in Figure 19 (a), which has instantaneous peak values of 10 kVDC. The corresponding line currents are shown in Figure 19 (b), and their RMS value is 1500 A.

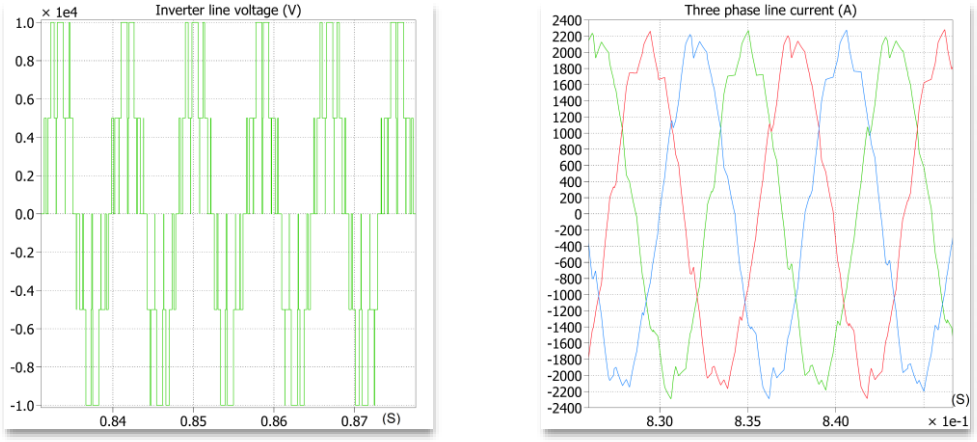

(a) Instantaneous Inverter Output Line Voltage (b) Three-phase Line Current

Figure 19. Inverter Output Line Voltage and Current

Because inverter mode is assumed in this simulation, the IGBT T_{1A}/T_{1B} (the upper-most ones in a leg) and T_{4A}/T_{4B} (the lower-most) will have highest losses and junction temperature. Thus T_1/T_4 will be the limiting devices in this situation. Waveforms for T_{1B} in steady state are shown in Figure 20 (a), including voltage across T_{1B}, current through T_{1B}, junction temperature T_j of T_{1B}, conduction losses and switching losses of T_{1B}. The waveforms show that the peak and average junction temperature of T_{1B} is 121°C and 111°C respectively. In addition, the total loss of T_{1B} is calculated as 7,082 W, including conduction loss 1,046 W and switching loss 6,036 W.

The diodes E2400EC45E work as clamping diodes in the circuit (D_{HA}, D_{HB}, D_{LA}, D_{LB} in Figure 17), and waveforms for D_{HB} in steady state are shown in Figure 20 (b). The waveforms show that the peak and average junction temperature of D_{HB} is 55.7°C and 55.3°C respectively. In addition, the total loss of D_{HB} is calculated as 1,378 W, including conduction loss 688 W and switching loss 690 W.

The simulation results reveal that junction temperature of the limiting devices T_{1B} (T2000BB45G) is below the maximum allowable junction temperature when working in the assumed simulation conditions, and the junction temperature of the clamping diodes D_{HB} (E2400EC45E) is well below the maximum allowable junction temperature.

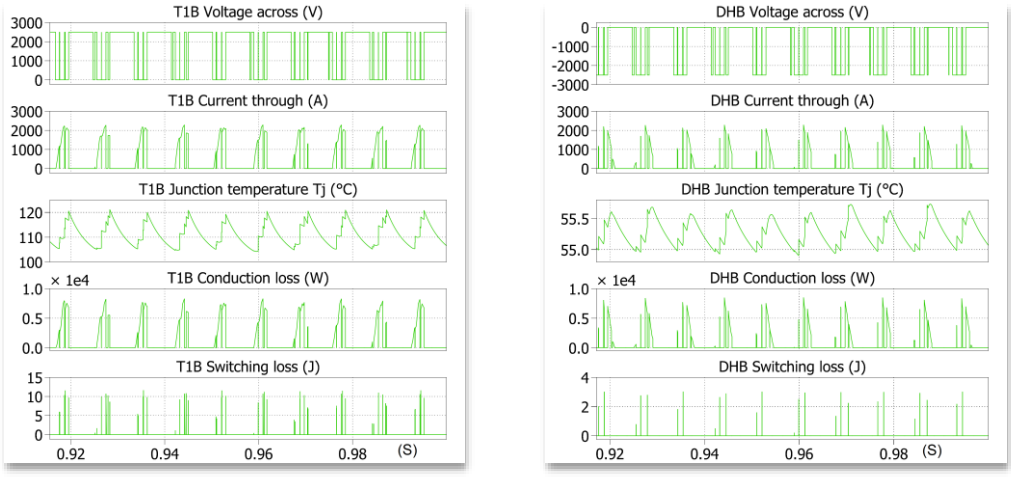

(a) IGBT T_{1B} (b) D_{HB} (E2400EC45E)

Figure 20. Simulation Results

4.2. Device Level Testing

Extensive tests have been carried out on PP-IGBT; only routine tests such as dynamic, RBSOA, short-circuit turn-off tests and type tests such as thermal cycling and short-circuit-failure-mode tests will be reported here.

4.2.1. Dynamic Test

Dynamic test is an important routine test for PP-IGBT, which is used to measure its dynamic parameters such as switching energy, turn on/off delay time, rise/fall time, turn on/off gate charges. The test circuit is shown in Figure 21 (a), and the double-pulse test procedure is used.

Typical waveforms of dynamic test for the 4.5 kV/2 kA PP-IGBT are shown in Figure 21 (b). The test was carried out under the following conditions: junction temperature T_j=125°C, DC-link voltage 2800 V, collector current I_C=2000 A, di/dt=3500 A/µs, and stray inductance L_S≈230 nH. From such waveforms, dynamic parameters of the 4.5 kV/2 kA PP-IGBT are obtained. Typical values are as follows: turn-on energy E_{on}=14J, turn-off energy E_{off}=12.5J, turn-on gate charge $Q_{g(on)}$=14.5 µC and turn-off gate charge $Q_{g(off)}$=11 µC [13].

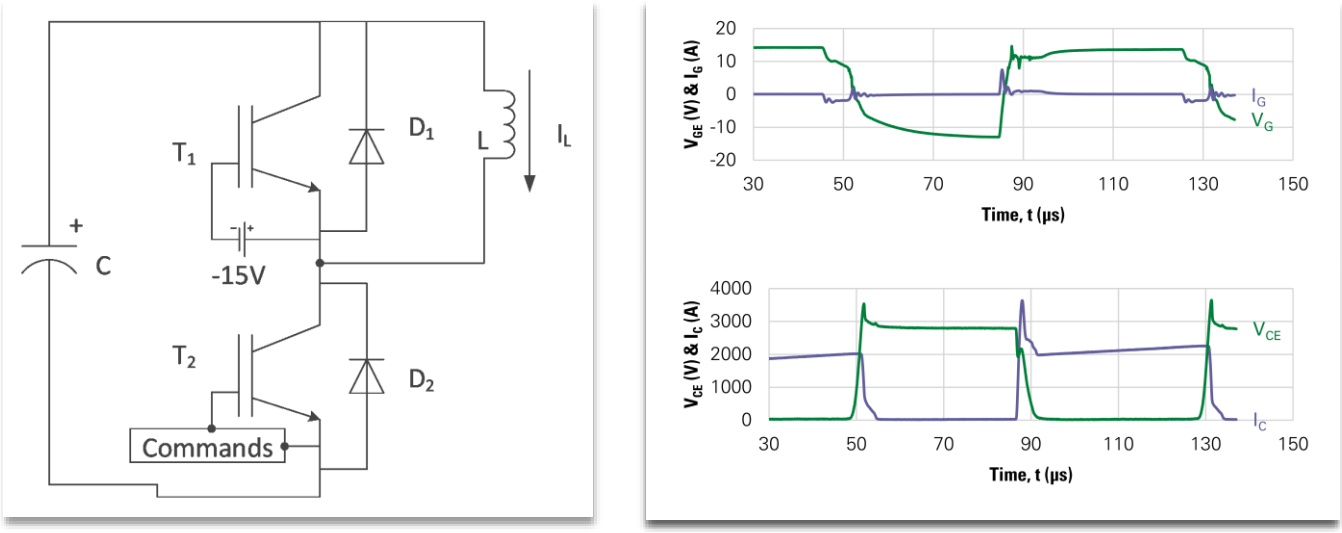

(a) Circuit Schematic

(b) Waveforms – T2000BB45G, T_j = 125 °C, V_{CE} = 2800 V, I_C = 2000 A, di/dt = 3500 A/µs

Figure 21. Dynamic Test for the 4.5 kV/2 kA PP-IGBT

4.2.2. Reverse Bias Safe Operating Area Tests

The Reverse Bias Safe Operating Area (RBSOA) test is a routine test for PP-IGBT. Its purpose is to define maximum switching locus of PP-IGBT. Its testing circuit is the same as the one for dynamic test (Figure 21 (a)), and its testing procedure is according to IEC 60747-9 [19]. Herein, a single pulse is applied to the 4.5 kV/2 kA PP-IGBT until the collector current I_C reaches 4 kA, and then a turn-off command is sent to the IGBT. The test was carried out under conditions of junction temperature T_j=125°C and DC-link voltage 2800 V, and the resulting waveform is shown in Figure 21.

.

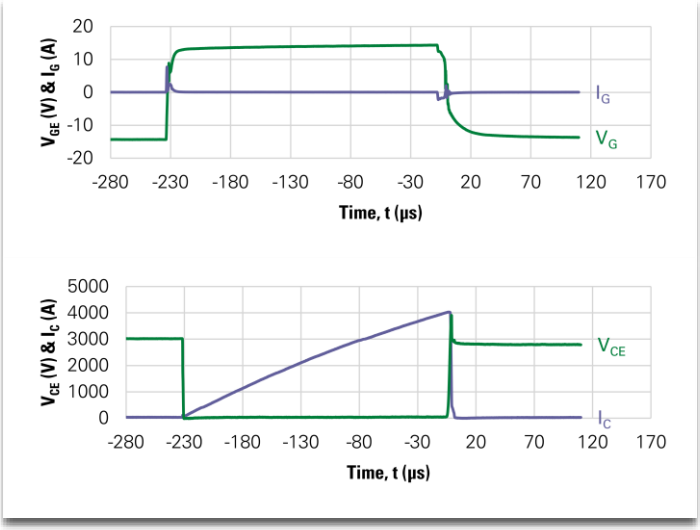

T2000BB45G, T_j = 125 °C, V_{CE} = 2800 V, I_C = 4000 A

Figure 22. RBSOA Test Waveforms

4.2.3. Short-circuit Turn-off Tests

This routine test is also known as type I short-circuit turn-off test [20], which is performed to verify that IGBT is able to turn off the short circuit current if shoot-through happens across the DC-link capacitor. The test circuit is shown in Figure 23 (a), where effectively the PP-IGBT under test is directly across the terminals of the DC-link capacitor. Prior to short circuit, a negative voltage (e.g. -15 V) is applied to the gate-emitter terminals, then gate-emitter voltage V_{GE} is switched to +15 V by a gate driver and shoot through of the DC-link capacitor happens during this turn-on process. As shown in the testing waveforms (Figure 23 (b)), the collector-emitter voltage V_{CE} starts to fall as collector current I_C goes up. However, because di/dt is quite high, very soon I_C becomes large enough to cause de-saturation. As a result, V_{CE} rises back to DC-link voltage. After 25 µs, the PP-IGBT is successfully turned off by applying -15 V on gate-emitter terminals. In this test, the DC-link voltage is 2800 V and starting junction temperature T_j is 125°C. The total energy during the short circuit process is measured to be 458 J and average power is approximately 17 MW, which proves the robustness of the PP-IGBT.

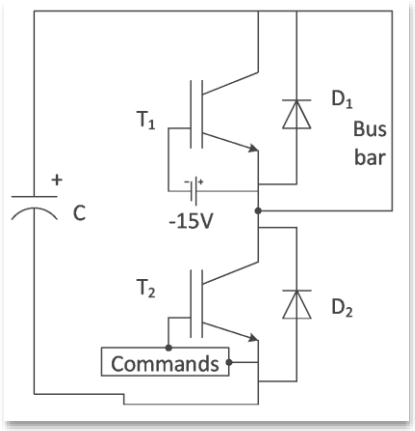

(a) Circuit Schematic

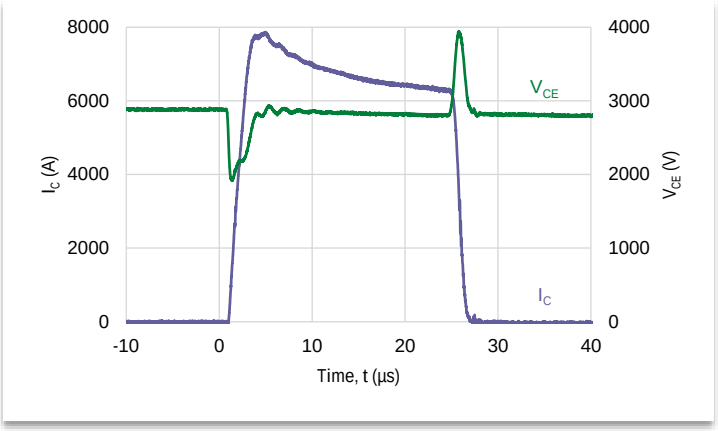

(b) Waveforms – T2000BB45G, short circuit switching test @ T_j = 125 °C, V_{CE} = 2800 V

Figure 23. Short-circuit Turn-off Test

4.2.4. Thermal Cycling Load Tests

This test is a type test, which is used to evaluate how PP-IGBTs cope with power cycling and thermal cycling. This type test was carried out on the 4.5 kV/2.4 kA PP-IGBT T2400GB45E [13] for 30,000 cycles, and three devices were tested together as a stack assembly (Figure 24 (a)). A cycle time of 2 minutes was used for the thermal cycling test (1 minute ON 1 minute OFF) and an average load of 1750 A. (Figure 25). Over each cycle the average case temperature of the hottest device varied from 79°C to 103°C, and junction temperature excursion is estimated to be approximately 90°C. The clamp force (max) varied from 62.0 kN to 70.9 kN. This variation in clamp force over the test duration is due to a combination of relaxation of the clamp components and variation in the temperature excursion.

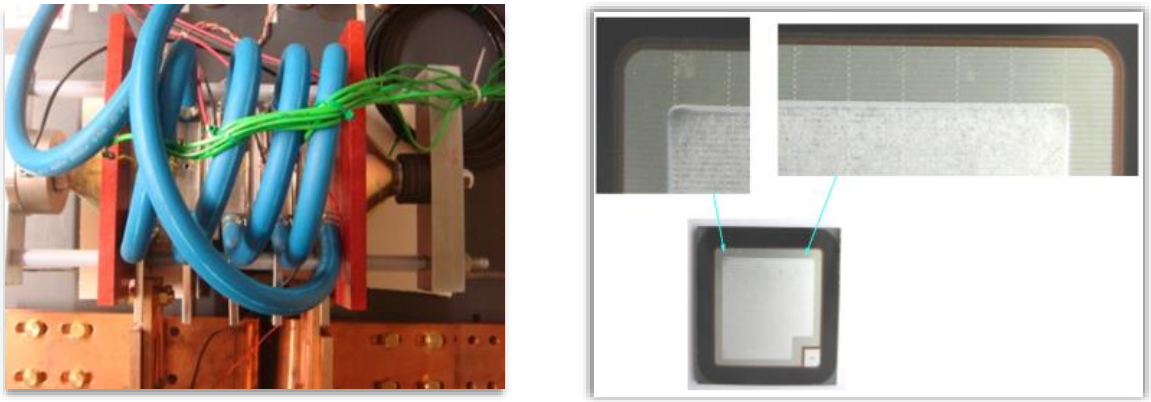

(a) Stack with Three Devices for Thermal Cycling Test

(b) Post Thermal Cycling Die Close up

Figure 24. Thermal Cycling Test

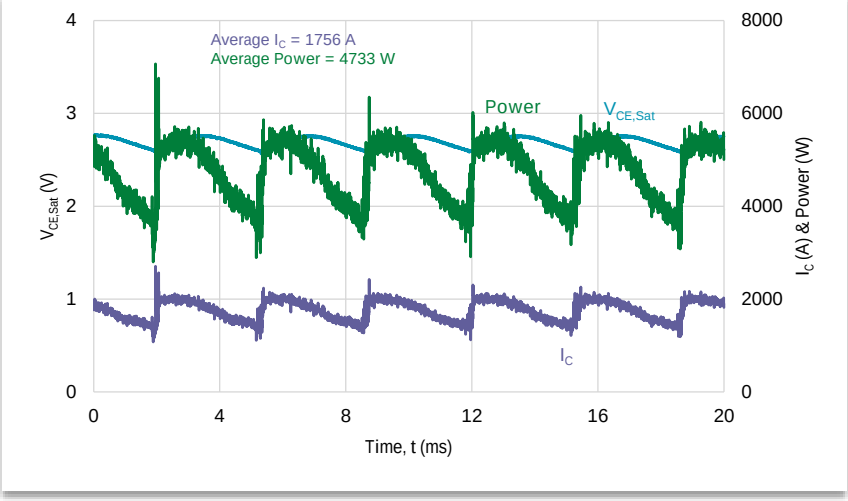

Figure 25. Power Input for Thermal Cycling Test

Static parameters of PP-IGBTs were measured before and after thermal cycling, and few changes were found according to the measurement results in Error! Reference source not found.. In addition, by opening the capsule of PP-IGBT after thermal cycling, the die shows minimal evidence of aluminum abrasion (Figure 24 (b)). Such tests prove that PP-IGBTs can withstand tough power and thermal cycling, and therefore have much longer lifetimes.

Table 7. Thermal Cycling Load Test (T_j = 125 °C)

Pre- or Post-Test	I_{GES} (**µA**)	I_{CES} (mA)	$V_{CE(SAT)}$ (V)	$V_{GE(TH)}$ (V)
Pre-test	4	17.8	3.52	5
Post-test	5	28.6	3.44	5.3

4.2.5. Short-circuit Failure-mode Tests

The press-pack IGBTs are ideally suited to applications where series operation is required. This quality is of particular interest for some MV drive applications where (N+1) redundancy is required. To ensure continued operation between maintenance cycles, it is essential that the device fails to a stable short circuit. An experiment has been conducted to observe this characteristic over a period of 8000 hours [12] and is reported in this application note.

This test is a type test, and it was carried out on the 4.5 kV/1.6 kA PP-IGBT T1600GB45G [13] that has built-in anti-parallel diode. Devices were prepared as follows: two samples with pre-damaged IGBT die and two samples with pre-damaged diode die. To proceed with the experiment, the devices were mounted in a series sub-assembly as shown in Figure 26 (a). Individual devices were mounted between copper coolers with a pressure sensing device included in the series stack, which can be seen at the left end of the stack in Figure 26 (a). To initiate the short circuit, each device was subject to a controlled capacitor discharge – a capacitor bank of 4 mF was charged to 4 kV and discharged through a 250 nH line inductance. Total energy discharge in the four devices was calculated as 16 kJ with a peak current of 357.8 kA.

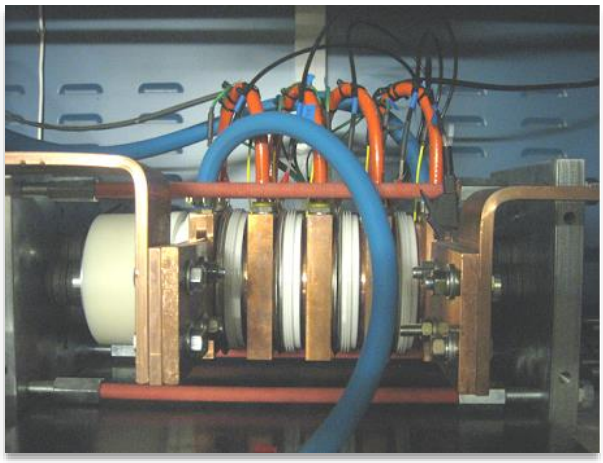

(a) Test Stack

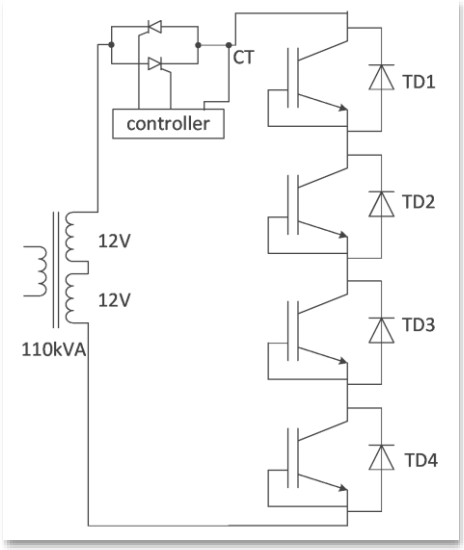

(b) Test Circuit

Figure 26. Short Circuit Test for (N+1) Redundancy

The stack was then mounted into the test fixture, with test circuit as shown in Figure 26 (b) [12]. An example of the current and voltage for TD_3 is given in Figure 27 (a) [12]. The test was continued for a period of 8000 hours with continuous monitoring. Current was monitored and controlled at 1200 A and the voltage drop across each device was recorded. Figure 27 (b) shows the output from the data logger for the four samples (voltage against time) over the full 8000-hour duration of the experiment. Some step changes in voltage drop were observed in the samples when the current flow in the equipment was removed to periodically measure any changes in a static condition. The worst case in TD_2 was observed with a variance of around 400 mV. However, during the running period of the test no device was observed to have a change in voltage drop of greater than ± 4%.

This experiment demonstrates the long-term stability of a short-circuit generated from a device failure and subsequent energy discharge in a press-pack IGBT. Once a stable condition was achieved, no significant change in the forward voltage drop across the device was observed over the complete test period of 8000 hours. The predictable and stable short circuit condition confirms the realistic application of an N+1 redundancy and the practicality in leaving the failed device in operation until the next planned maintenance cycle.

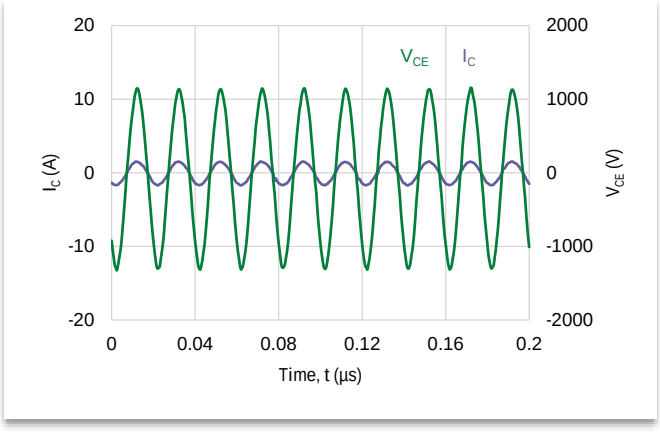

(a) Typical Power Waveforms

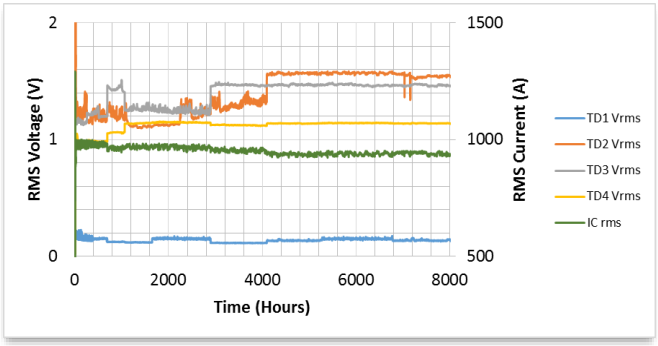

(b) Data Logger Output over 8000 hours

Figure 27. Long-term Stability Test from Short-circuit Generated by Device Failure

4.1. Stack Tests

Commutation and frequency tests are two essential tests for submodules, which are presented here.

4.1.1. Double-pulse Commutation Tests

During the commutation test, IGBTs are turned ON and OFF, and waveforms for both IGBT and freewheeling diodes are recorded. Such waveforms can then be analyzed to evaluate if the IGBT V_{CE} turn-off voltage and diode reverse recovery are inside their Safe Operating Area (SOA), to assess suitability of gate driver parameters, and to check for unwanted oscillations. In addition, series operation of power devices is involved in this project and therefore, close attention is paid to the dynamic sharing issue.

The commutation test circuit for low side switching is shown in Figure 28 (a), where the inductive load is connected between the DC plus terminal and the AC output terminal. During this test, the IGBT T_{1A} and T_{1B} are kept OFF all the time, and the IGBT T_{3A} and T_{3B} are kept ON all the time. The double pulse testing procedure will be applied to the IGBT T_{4A} and T_{4B}, and gate signals to T_{2A} and T_{2B} are essentially inverted ones to those of T_{4A} and T_{4B} but with certain blank time. Figure 28 (b) shows the stacks and test setup.

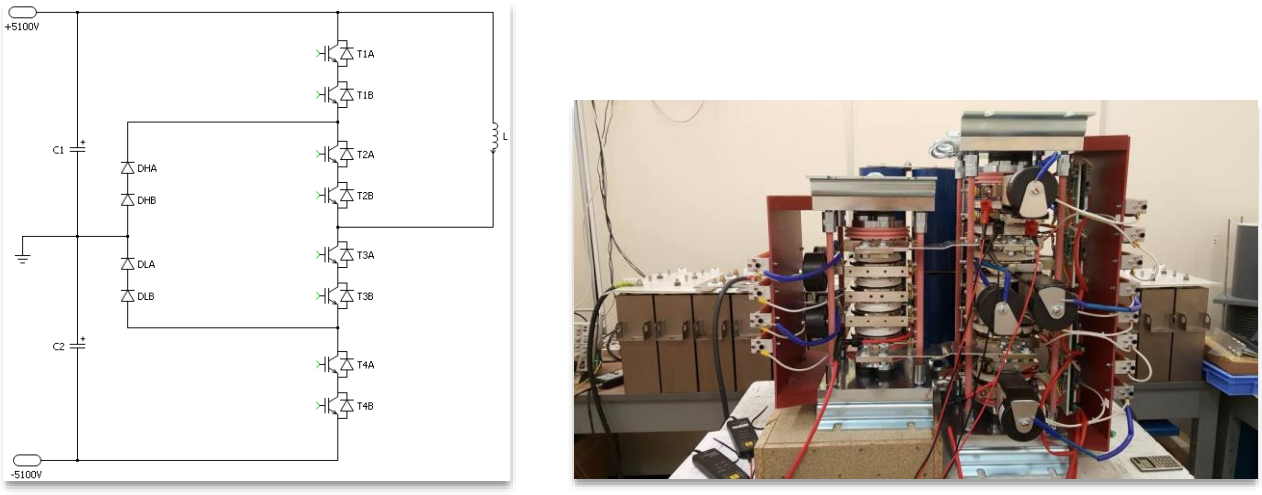

(a) Circuit (b) Setup

Figure 28. Commutation Test

The test was carried out at room temperature, and the DC-link voltage is ±5100 V. Test waveforms for IGBT T_{4A} and T_{4B} are shown in Figure 29 (a), which shows that dynamic voltage sharing between T_{4A} and T_{4B} during switching is very good, and static sharing after turn-off is reasonable. In the test, the collector current I_C is turned OFF at the value of 2165 A, and the corresponding peak value of the collector-emitter voltage V_{CE} of T_{4A} is 3308 V, which results in an overshoot voltage of 686 V.

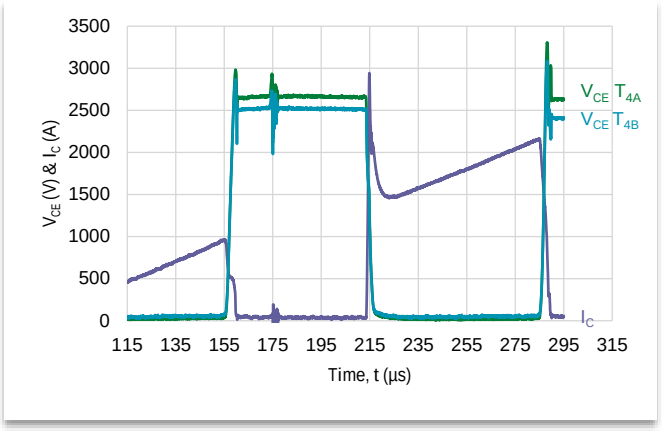

(a) IGBT T_{4A} and T_{4B} – T_j = 25 °C, DC-link ±5100 V

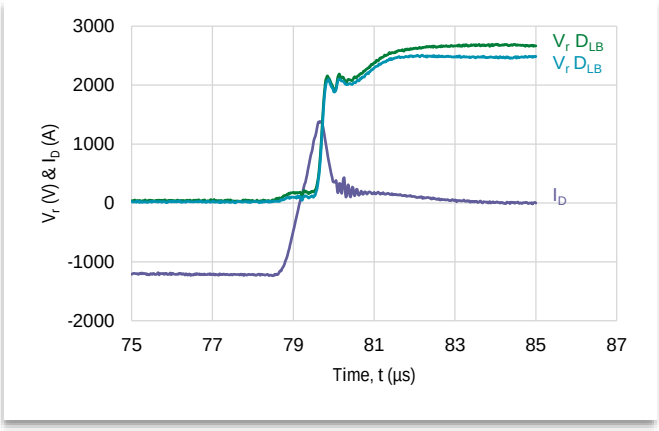

(b) Diode D_{LA} and D_{LB} – Clamping Diode, T_j = 25 °C, DC-link ±5100 V

Figure 29. Test Waveforms

When IGBTs T_{4A} and T_{4B} are turned ON, the load current will be commutated from the clamping diodes D_{LA} and D_{LB} to T_{4A} and T_{4B}. Test waveforms for D_{LA} and D_{LB} during the commutation are shown in Figure 29 (b), which illustrates that both dynamic and static voltage sharing between diode D_{LA} and D_{LB} are good. The freewheeling current in the diodes before commutation is approximately 1200 A, and the peak reverse recovery current is around 1383 A. The diode peak recovery power is about 2.13 MW, which is well inside its SOA [14]. Moreover, the diode current I_d shows a very good soft recovery curve, which effectively prevents potential oscillations and snappy behaviors.

4.1.2. Frequency Tests

The frequency test is also known as the thermal stability test or leg test. It is designed to confirm that power semiconductor switches are capable of operating stably at nominal load and overload conditions, free from thermal runaway or undesired lifetime reduction. Frequency tests also provide opportunities to assess power devices' commutation capabilities in continuous operation, to verify stack cooling design, and to measure power losses. Therefore, this is an important test for stack design of submodules. The test circuit, testing procedure, and test rig setup are detailed in [21], and the test circuit is redrawn in Figure 30 (a).

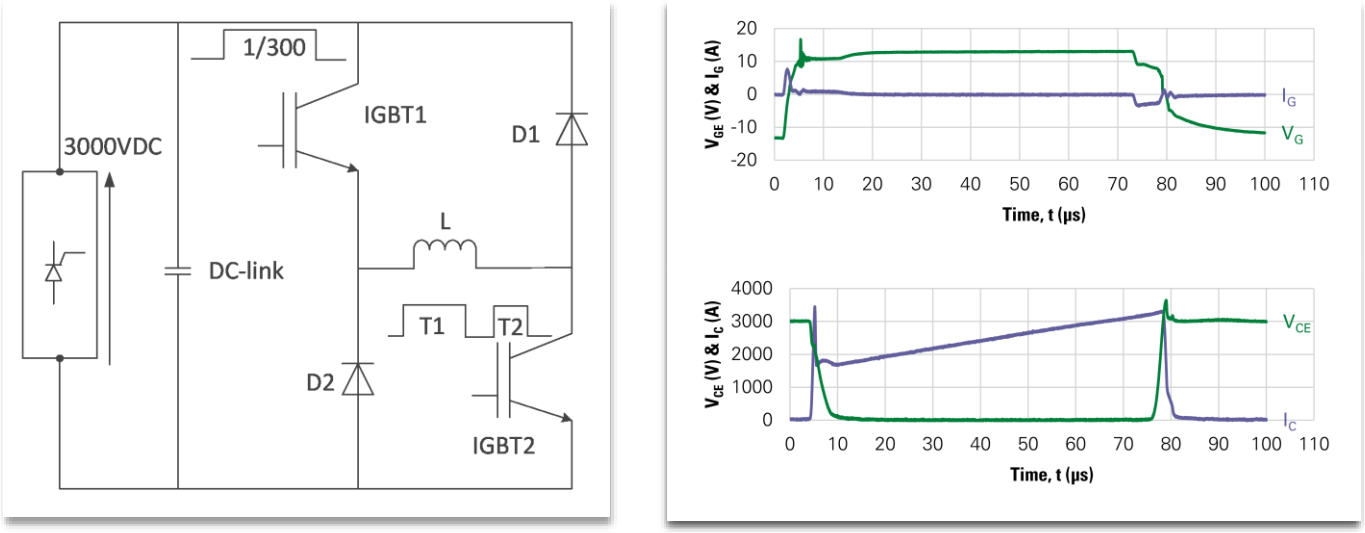

(a) Circuit

(b) Waveforms – Frequency Switching, T2960BB45E, V_{CE} = 3000 V, I_C = 3350 A @ 300 Hz

Figure 30. Frequency Test

Due to voltage limitation of the in-house test rig, the frequency test has not been carried out on this 6.6 kV phase leg assembly. However, for completeness, the frequency test results for another stack using the PP-IGBT T2960BB45E are reported here. The stack for the submodule is tested with incremental load current, for a total test period of 10 minutes at each testing point. Figure 30 (b) shows testing waveforms with I_C current of 3350 A. This test was performed with DC-link capacitor voltage at 3000 V and switching frequency at 300 Hz. It demonstrates that cooling design is efficient enough to take away power losses of power devices, so that the stack for the submodule can operate stably at the required load conditions. In addition, switching capabilities of power devices in continuous operation are also validated.

By measuring and recording coolant flow rate and inlet and outlet temperatures, the total losses of the stack can be calculated. Additionally, average junction temperature of PP-IGBT can be derived using a thermal equivalent circuit, if both its electrodes' temperatures are measured [22].

5. Summary

VSC MV drives play an important role in many areas, and fully controllable power switches, normally IGBTs, are essential devices for the power stage of MV drives. PP-IGBT is a specialty IGBT with high reliability and power density, making PP-IGBT based MV drives a primary choice for various critical applications such as marine propulsions, offshore wind turbines, gas compressors and steel mills.

Common and emerging topologies for MV drives were reviewed in this application note, and the structure and features of PP-IGBT were discussed. The design, analysis, and testing process of a 3L-NPC MV drive using PP-IGBTs with a rating of 6.6 kV/16 MVA was also presented.

6. References

[1] B. Wu, High-Power Converters and AC Drives, Hoboken, New Jersey, John Wiley & Sons, Inc., 2006
[2] H. Liu & J. Jiang. & W. Luo (2015). A comparative analysis of the three-level NPC and ANPC converter loss distribution. Journal of Electrical Systems. 11. 271-280
[3] O. S. Senturk, L. Helle, S. Munk-Nielsen, P. Rodriguez and R. Teodorescu, "Converter Structure-Based Power Loss and Static Thermal Modeling of The Press-Pack IGBT Three-Level ANPC VSC Applied to Multi-MW Wind Turbines," in IEEE Transactions on Industry Applications, vol. 47, no. 6, pp. 2505-2515, Nov.-Dec. 2011
[4] M. Schweizer and J. W. Kolar, "Design and Implementation of a Highly Efficient Three-Level T-Type Converter for Low-Voltage Applications," in IEEE Transactions on Power Electronics, vol. 28, no. 2, pp. 899-907, Feb. 2013
[5] N. Binesh, "Understanding the Latest in MV Drive Topologies", Regal Beloit Corporation, Nov 2017
[6] "Multilevel Technology with ALSPA VDM6000", http://power-conversion.enseeiht.fr/DCAC/Xlevel_Technology_with_VDM6000.pdf, accessed 12 Mar 2020
[7] R. Marquardt, "Modular Multilevel Converter: A universal concept for HVDC-Networks and extended DC-Bus-applications," The 2010 International Power Electronics Conference - ECCE ASIA -, Sapporo, 2010, pp. 502-507
[8] IEC/TR 625431: "High-voltage direct current (HVDC) power transmission using voltage sourced converters (VSC)", Edition 1.0, 2011-03
[9] G. Postiglione, G. Borghetti, G. Torre, and P. Bordignon, "Transformerless STATCOM based on multilevel converter for grid voltage restoring", International Exhibition and Conference for Power Electronics, Intelligent Motion, Power Quality. PCIM Europe 2011, p413-19, 2011
[10] F. Wakeman, et al, "Electromechanical characteristics of a bondless pressure contact IGBT," Applied Power Electronics Conference and Exposition, 1999. APEC '99. Fourteenth Annual, Dallas, TX, 1999, pp. 312-317 vol.1
[11] A. Golland & F. Wakeman "New family of 4.5 kV Press-pack IGBTs", PCIM 2005, pp 137 – 142
[12] F. Wakeman, J. Pitman and S. Steinhoff, "Long term short-circuit stability in Press-pack IGBTs," 2016 18th European Conference on Power Electronics and Applications (EPE'16 ECCE Europe), Karlsruhe, 2016, pp. 1-10
[13] "Capsule Type Series - Press-Pack IGBT", https://www.littelfuse.com/products/power-semiconductors/discrete-igbts/high-power-igbts/capsule-type.aspx, accessed 12 Mar 2020
[14] "HP Sonic FRD Series - High Power Sonic FRD", https://www.littelfuse.com/products/power-semiconductors/discrete-diodes/fast-recovery/hp-sonic-frd.aspx, accessed 12 Mar 2020
[15] Q. Al-Akayshee, H. Neal, et al, "Semiconductor Devices Used in Heavy Duty Industrial Applications", 2018 IET 9th International Conference on Power Electronics, Machines & Drives (PEMD), Liverpool, UK, 2018
[16] "Coolers Series - Capsule Water Coolers", https://www.littelfuse.com/products/power-semiconductors/stacks-subsystems-and-assemblies/accessories/coolers.aspx, accessed 12 Mar 2020
[17] Q. Al'Akayshee, H. Neal, A. Sartain, S. Reynolds, X. Yuan and M. Al'Akayshee, "AN 8 MW, 3-level inverter drive based on presspack IGBT's: Design, construction and operational propulsion system," 8th IET International Conference on Power Electronics, Machines and Drives (PEMD 2016), Glasgow, 2016, pp. 1-6
[18] "Clamps Series - Standard Bar Clamps", https://www.littelfuse.com/products/power-semiconductors/stacks-subsystems-and-assemblies/accessories/clamps.aspx, accessed 12 Mar 2020
[19] IEC 60747-9: "Semiconductor devices – Discrete devices – Part 9: Insulated-gate bipolar transistors (IGBTs)", Edition 2.0, 2007-09
[20] J. Fuhrmann, D. Hammes and H. G. Eckel, "Short-circuit behavior of high-voltage IGBTs," IECON 2016 - 42nd Annual Conference of the IEEE Industrial Electronics Society, Florence, 2016, pp. 1165-1170
[21] G. Li, F. Wakeman, J. Whitby, Q. Al'Akayshee, "Test procedure to ensure quality of 4.5 kV very high current Press-Pack IGBTs", PCIM 2008, V3
[22] H. Chen, W. Cao, P. Bordignon, R. Yi, H. Zhang and W. Shi, "Design and testing of the World's first single-level press-pack IGBT based submodule for MMC VSC HVDC applications," 2015 IEEE Energy Conversion Congress and Exposition (ECCE), Montreal, QC, 2015, pp. 3359-3366